Journal of The
Electrochemical Society

Ultrasensitive Screen-Printed-Electrodes for p-aminophenol Analysis and Applications in Bioremediation and Photodegradation Processes

To cite this article: Jean-Philippe Théodore Silga *et al* 2025 *J. Electrochem. Soc.* **172** 027501

Journal of The Electrochemical Society, 2025 **172** 027501

Ultrasensitive Screen-Printed-Electrodes for p-aminophenol Analysis and Applications in Bioremediation and Photodegradation Processes

Jean-Philippe Théodore Silga,[1,2] Serge Mbokou Foukmeniok,[1] Yibor Fabrice Roland Bako,[2,3] Assia Chaouch Ramdane,[4] Maryam Nazerifar,[5] Habibollah Younesi,[5] Issa Tapsoba,[2] and Pontié Maxime[1,z]

[1]*Group of Analysis and Processes (GA&P), Department of Chemistry, University of Angers, 49045 Angers Cedex 01, France*
[2]*Laboratoire de Chimie Analytique, Environnementale et Bio-Organique (LCAEBiO), Université Joseph KI-ZERBO, 03 BP 7021 Ouaga 03, Burkina Faso*
[3]*Laboratoire Interdisciplinaire de Recherche en Sciences Appliquées (LIRSA), Ecole Normale Supérieure, 01 BP 1757 Ouagadougou 01, Burkina Faso*
[4]*Laboratoire de chimie inorganique et environnement, University Abou Bekr Belkaid, 113 BP, Tlemcen, Algeria*
[5]*Department of Environmental science, Faculty of Natural Resources, Tarbiat Modares University, Noor, Iran*

A screen-printed electrode (SPE) was successfully activated and modified by electrodeposition of nickel (II) tetrasulfonated phthalocyanine film (poly-NiTSPc) for the electrochemical analysis of para-aminophenol (PAP). Cyclic voltammetry, differential pulse voltammetry, electrochemical impedance spectroscopy, optical microscopy and scanning electron microscopy coupled with energy dispersive X-ray (EDX) experiments were performed to characterize the SPE. Calibration curves were determined in the concentration range of 0.1 mg l^{-1} to 2.4 mg l^{-1} using the tested electrodes and linear relationships were resolved between peak current intensities and PAP concentrations. The limits of detection (LOD) obtained were 74 μg l^{-1}, 34 μg l^{-1}, 29 μg l^{-1} and 26 μg l^{-1} for unmodified SPE, poly-NiTSPc/SPE, activated/SPE and poly-NiTSPc/activated SPE, respectively. The poly-NiTSPc/activated SPE was applied for the bioremediation study of PAP using *Trichoderma harzianum* in a fungal microbial fuel cell (MFC). Our results showed a first-order kinetic degradation with a kinetic constant of 0.063 h^{-1} at 20 °C and a half-time of degradation of 11 h for an initial concentration of 100 mg l^{-1}. Subsequently, we assessed the poly-NiTSPc/activated SPE for PAP identification as a by-product of crystal violet degradation in a photocatalytic system using Ag/$FeVO_4$ as a photocatalyzor in the presence of H_2O_2.

 [DOI: 10.1149/1945-7111/adada5]

Manuscript submitted July 13, 2024; revised manuscript received December 31, 2024. Published February 3, 2025.

Para-aminophenol (PAP) is a synthetic raw material widely used in numerous industrial sectors with applications in resin, rubber, explosives, pesticides, textiles, and in the production of dyestuffs to dye materials such as hair, fur, feathers and wood.[1] This intensive use of PAP could justify its large distribution in environmental matrices. Also, it is well known that PAP is the main bacterial biodegradation by-product of paracetamol and has been frequently detected in hospital wastewater. Notably, PAP has been confirmed as genotoxic, mutagenic and hepatotoxic with its facile penetration through the skin and membranes of humans, animals, and plants an indicator of its harmful effects.[2] Therefore, the monitoring of PAP levels in different matrices has become an important environmental challenge. Up to now, conventional analytical techniques such as gas/liquid chromatography,[3] capillary electrophoresis,[4] microfluidic devices,[5] and spectrophotometry[6] are generally used for PAP determination. However, some of these methods have drawbacks, such as long operation time, high cost, and low sensitivity.[7] These limitations mean they are not ideal for rapid and routine analysis. Besides their analytical performance in terms of sensitivity, electrochemical techniques offer the advantages of being economical, portable, reliable, and rapid for the detection of toxic molecules.[8–11] These methods are important in biological and environmental analysis because of these unique properties and the ability to enable on-site and real-time detection[12,13] Electrochemical sensors based on carbon materials such as carbon nanotubes, graphene, graphite, and carbon nanofibers have been utilized in environmental detection due to their unique features in terms of large specific surface area, rapid electronic transmission, and good biocompatibility.[14,15] Moreover, these sensors can be modified via the addition of a molecule or compound on its surface that displays a strong affinity with the analyte. The aim of this modification is to increase the sensitivity of the electrode by reducing the limit of detection.[16] For instance, classic three electrodes system (reference, auxiliary and working electrode) are widely used for electrochemical analysis. This includes the use of an electrochemical cell with a large volume of analyte solution, which is not suitable for on-site analysis, hence the need to move towards other types of electrodes such as screen-printed electrodes (SPEs). Recently, SPEs have attracted considerable attention for the development of electrochemical sensors owing to their numerous advantages including simple fabrication, small size, low cost, portability, large-scale production, availability, reproducibility, and sensitive real-time detection of an analyte without any pre-treatment.[17] SPEs consist of printing conductive inks (e.g. carbon, platinum, gold, or silver inks) onto a solid substrate, combining the conventional three electrodes system into one solid surface[17,18] They require just a few microliters (60 μl) on their surface for analysis and are suitable and adapted for on-site analysis. As for classical electrodes, SPE surfaces can be modified with the aim of increasing their sensitivities. Several materials are being used as modifiers for increasing the electrical conductivity of electrodes including nickel(II) tetrasulfonated phthalocyanine complex (NiTSPc) has shown promising results. Mbokou et al. modified an ultramicroelectrode with poly-NiTSPc for quality control analysis of diuron in commercial formulation.[19] Bougna et al. developed a sensor based on poly-NiTSPc combined with gold nanoparticles for butylhydroxyanisole analysis in water.[20] More recently, Bako et al. proposed the modification of an ultramicroelectrode with poly-NiTSPc for indirect determination of 3-methyl-4-nitrophenol.[21] These studies demonstrate that poly-NiTSPc significantly improves electrode performances for pollutant analysis. In addition, Raymmundo-Pereira et al. showed that the activation of SPEs in H_2SO_4 leads to superior electron transfer during electrochemical reactions.[22]

[z]E-mail: maxime.pontié@univ-angers.fr

Beyond the detection of pollutants, of interest is identifying an eco-friendly process for their bioremediation.[23] In fact, opportunity lies in wastewater remediation especially the degradation of different types of organic micropollutants.[24] PAP is known to be released into the aquatic environment via various resources of chemical processes, hospital and industry effluents. Developing a low-cost and environmentally friendly process for efficient removal of PAP from wastewater is a priority. Up till now, various approaches have been used for PAP degradation. Ratiu et al. proposed the degradation-based photocatalytically-assisted electrochemical for PAP in aqueous solutions by zeolite-supported TiO_2 catalyst.[25] Tewari et al. studied PAP removal from water based on lead, bismuth, and manganese ferrocyanide adsorption.[26] However, they do not lead to the total removal of the pollutant and hazardous by-products are generated. The use of fungi and their enzymes for pollutant removal has been well established in the literature.[27] Microbial fuel cell (MFCs) are bioelectrochemical systems that utilize the enzymatic activity of microorganisms for pollutant removal while simultaneously generating energy. The microorganism used in this study is *Trichoderma harzianum (T. harzianum)* whose enzymes such as laccase exhibit the ability to oxidize a large range of chemical compounds without the generation of by-products.[28,29]

Herein, we present a SPE activated in H_2SO_4 and then modified with nickel (II) tetrasulfonated phthalocyanine (poly-NiTSPc) for ultrasensitive analysis of PAP in aqueous solution. The proposed sensor was first applied to study the PAP bioremediation in MFC using *T. harzianum* fungus.

Subsequently, a crystal violet (a dye widely used in industry) degradation study was conducted using an advanced oxidation process: photodegradation. The sensor was then employed to demonstrate the formation of PAP as a by-product generated during the photodegradation process of crystal violet (Cv).

Materials and Methods

Reagents and materials.—Para-aminophenol, Nickel (II) tetrasulfonated phtalocyanine, acetic acid, sodium acetate, and sulfuric acid were purchased from Sigma Aldrich (France) and used as received. Acetate buffer solution (ABS, pH = 5, ionic strength 0.1 M) used as supporting electrolyte was obtained from the following reagents: $C_2H_4O_2$ and $C_2H_4O_2Na$. $3H_2O$. Both reagents were purchased from Merck Company (France). All aqueous solutions were prepared from analytical grade chemicals, using ultra-pure water.

Apparatus.—Electrochemical measurements were carried out on an EmStat 4X electrochemical analyser (PalmSens Instruments, France) running with the PS trace software and connected to a personal computer. A three-component DropSens screen-printed electrode (DRP-110, Spain) consisting of a graphite working electrode, a silver pseudo-reference electrode, and a graphite counter electrode was used for electrochemical measurements. Electrochemical impedance spectroscopy (EIS) measurements were performed using Origaflex potentiostat purchased from Origalys company (Lyon, France) controlled by a computer using OrigaMaster 5 as software. Images and roughness of the SPEs surface were recorded using a digital microscope (Keyence VHX) for a magnification of $\times 100$ in a window of 6 mm^2. For carbon cloth observation, scanning electron microscopy (SEM) was also used using a field emission gun scanning electron microscopy (FESEM) on a JSM-6301 F apparatus from JEOL (SCIAM, Angers University, France). All figures and graphs were plotted using ORIGIN software (license N° GA&P laboratory (UA): GF3S5-6089-7183940).

Electrochemical sensors development.—The activation of SPE was carried out in H_2SO_4 (0.5 M) by sweeping in cyclic voltammetry at a scan rate of 100 mV s^{-1} and for two cycles from −2.5 to 2.5 V Ag^{-1}.[22] The activation aimed to remove residues, adhesives, or oils that might have accumulated on the SPE surface during the manufacturing process and also to improve the electron transfer rate on the working electrode surface enhancing sensing performance and hydrophilicity of SPEs as reported in the literature.[30] Poly-NiTSPc film deposition was initiated with a first step which consisted of recording 5 successive cyclic voltammograms on unmodified SPE (for poly-NiTSPc/SPE elaboration) and on activated-SPE (for poly-NiTSPc/activated SPE elaboration) in the presence of 0.1 M NaOH at the scan rate of 100 mV s^{-1}.[31] The aim of this step is to generate oxygen functional groups on SPE surface which is essential for poly-NiTSPc deposition. Following this step, poly-NiTSPc was electrodeposited by performing 75 cyclic scans in 2 mM NiTSPc solution prepared in 0.1 M NaOH. The number of cycles is adapted from a previous study which reported that the high electrocatalytic effect of poly-NiTSPc film is observed at 75 scans.[21]

Electrochemical measurements.—Cyclic Voltammetry (CV) at a scan rate of 100 mV s^{-1} was used for electrochemical characterizations of the elaborated SPEs and poly-NiTSPc film deposition. In contrast, differential pulse voltammetry (DPV) was used for determination of PAP with the following optimized parameters: Step potential 5 mV, pulse potential 50 mV, and pulse time 20 ms (results not shown). The appropriate volume of solution placed on the SPE surface before each analysis was set to 60 µl. All electrochemical measurements were made at room temperature.

Microorganism.—*T. harzianum* strain 918 used in this study was provided by IRHS-INRAE Angers France. The fungi stock culture was prepared on a Potato Glucose Agar (PGA) plate containing 5 g l^{-1} of potato extract, 20 g l^{-1} of dextrose and 15 g l^{-1} of agar (Sigma Aldrich). The strain was then maintained at 4 °C.

T. harzianum is an ascomycete fungus, non-pathogenic to human and the environment and widely used for pollutant removal.[29,32] Due to its enzymatic activity, *T. harzianum* could efficiently cleave double C=C bonds of aromatic compounds leading to a bioremediation.

Bioanode elaboration.—Carbon cloth CC (DACARB TIS_KIP_1300, France) was used as the electrode material (9 cm^2) in both the anode and cathode compartments. The anode should provide ideal conditions for the microorganism to facilitate the degradation of pollutant. Before use, CC was cleaned using the protocol already reported[23,29,33] and then used as a supporting layer for biofilm deposition. For that, CC was immersed into a prepared suspended solution of fungi and acetate buffer solution (0.1 M, pH = 4.8) under agitation for three days. The experiment was carried out in microbiological safety conditions to avoid any external contamination. After these three days, a mature biofilm was obtained on CC and then used as the bioanode in the MFC.

Biocathode elaboration.—CC 9 cm^2 of geometrical area (DACARB TIS_KIP_1300, France) was cleaned using the same protocol used for the anode cleaning. After, the CC without any modification was immersed into the cathodic compartment containing potassium ferricyanide (10 g l^{-1}) in an acetate buffer solution (0.1 M pH = 4.8). Many authors demonstrated that adding potassium ferricyanide in the cathodic compartment aimed to catalyse O_2 reduction and improve MFC performances.

Fungal strain preparation protocol for SEM observation.—CC modified with *T. harzianum* mycelium and unmodified CC were observed using SEM. Before the observation, all samples were first immersed in 2.5% of glutaraldehyde and 2.5% of paraformaldehyde in cacodylate buffer for the fungi fixation, after the samples were subjected to osmium tetraoxide treatment followed by dehydration in ethanol and then in hexamethyldisilasane. The samples of CCs were then deposited on a steel disk and then covered with an ultrathin layer of platinum before being placed into the SEM chamber for observations.

Membrane elaboration.— *Preparation of sulfonated polyethersulfone polymer.*—The process of sulfonation of the polyethersulfone (PES) sample was carried out following the method described by Lu et al.[34] First, the PES (BASF Co, Germany) flakes were dried overnight at 80 °C in a vacuum oven. Next, 10 g of PES flakes and 100 ml of concentrated sulfuric acid were mixed in a three-necked glass flask, equipped with a reflux condenser, and stirred vigorously for 24 h at room temperature until the polymer was completely dissolved. In the next step, 50 ml of chlorosulfonic acid was gradually added to the above solution under an N_2 atmosphere and continuous stirring, while agitated for another 30 min. The reaction mixture was kept at 10 °C for 32 h. After, the sulfonated PES (sPES) was precipitated into a large volume 100 ml of ice-cold deionized water, and then washed with deionized water until the pH became neutral (∼6–7). Finally, the resulting polymer was dried under vacuum at 60 °C for 24 h.

Synthesis of hyper-crosslinked polymers.—The hyper-crosslinked polymers (HCPs) were produced using a method described in the literature.[35] First, anhydrous $FeCl_3$ (1.3 g, 8 mmol) was added to a solution of phenol (0.35 g, 4 mmol) and FDA (0.7 ml, 8 mmol) in 12 ml of 1,2-dichloroethane (DCE). The mixture was then stirred for 18 h at 80 °C. After the reaction was quenched with MeOH 10 ml, the resulting polymer was filtered and washed with MeOH and water. The solid was then purified using soxhlet extraction with MeOH for 24 h followed by drying under vacuum at 70 °C for 12 h.

Sulfonation of HCPs.—The as-synthesized HCPs (1.50 g) were added to 50 ml of DCE and stirred for 1 h to allow the polymer network to swell in the solvent. Then, 10 ml of chlorosulfonic acid were added to the solution and stirred at 25 °C for 72 h. The resulting product was collected via vacuum filtration and washed with neutral pH water and methanol. Finally, the solid was dried under vacuum at 60 °C overnight, resulting in the final black product with yields of 1.70–1.96 g for sulfonated HCP (sHCP).

Fabrication of sPES/sHCP composite membranes.—The sPES/sHCP membranes were fabricated using the dry-phase inversion method. To start, a specific amount of sulfonated sHCP polymer (0.01, 0.02, 0.03, and 0.04 g) was dissolved in dimethylacetamide (DMAc Merck, Germany), designated as solution A. Simultaneously, the exact amount of sPES was dissolved in DMAc (0.5 g), designated as solution B. Then, both solutions were stirred for 24 h at 150 rpm to ensure thorough mixing. Solution A was added dropwise into solution B, and the mixture was continuously agitated until a clear solution was obtained and later stirred for 3 h. The mixture was then sonicated for 10 min to remove any trapped dissolved air bubbles. A clear and homogeneous solution of sPES/sHCP was then cast on a clean flat glass using a casting knife with different thicknesses The thickness of the dried membrane after 24 h in the oven at 70 degree C was 63–68 μm. For your information, we fabricated three different thickness of membranes using a casting knife, adjusting its thickness to 160, 180, and 200 μm. The membrane used in the present study has a thickness of 200 μm due to its better performances in microbial fuel cell (results not shown).

Afterwards, it was air-dried at room temperature for 3 h, followed by oven heating at 70 °C for 24 h and annealing at 100 °C for 8 h. After the flat sheet membrane had cooled to room temperature, it was soaked in deionized water and then peeled off from the glass plate. The membrane samples were named sPES/sHCPx−y, where *x* is the membrane thickness and *y* is the weight percent of sHCP. Subsequently, the membrane was shaped into a ring with a diameter of approximately 5 cm, treated with 1 M H_2SO_4 for 12 h, and then stored in deionized water for future use.[36] Table I shows the chemical composition of the as-prepared membranes using various sHCP and sPES amounts with different thicknesses.[37]

Membrane cationic exchange capacity (CEC) determination.—The CEC of the elaborated membrane was determined following the method described by Somrani et al.[38] ∼0.160 g of the membrane was immersed into 1 M HCl for 24 h and then rinsed in ultrapure water. The membrane was then dried in a desiccator for 48 h and weighed. The membrane was then immersed into 50 ml of NaCl (2 M) for 24 h. NaOH (1 M) was used to titrate NaCl solution using phenolphthalein as indicator for neutral point determination. CEC was then calculated using the following equation.[38]

$$\mathrm{CEC} = \frac{\mathrm{MV}}{W} \qquad [1]$$

Where M and V are molar concentration and volume (ml) of NaOH, respectively and W the weight of dried membrane (g)

MFC setup and operation.—The MFC used in this experiment consisted of two compartments, an anode and a cathode, separated by a self-elaborated proton exchange membrane. The role of the membrane is to allow protons to transfer from the anodic chamber to the cathodic chamber while preventing the mixing of the two compartments. Both compartments were sterilized via autoclaving and assembled in microbiological safety conditions. The working volume for each compartment was 50 ml. The anodic compartment was filled with 100 mg l^{-1} of PAP in an acetate buffer solution (0.1 M pH = 4.8) in which a carbon cloth covered by the biofilm of *T. harzianum* was immersed. The cathodic chamber contained potassium ferricyanide (10 g l^{-1}) in acetate buffer solution (0.1 M pH = 4.8). The two carbon cloths type KIP-1300 (KIP) carbon clothes electrodes are gracefully given by Dacarb (Asnières-sur-Seine, France) and are connected to the electrical circuit via platinum rods and alligator clips. The circuit consisted of a multimeter to follow electromotive force EMF vs time and a resistance decade box (10 MΩ ∼ 1 kΩ) arranged in parallel for optimal resistance and power density determinations. Dioxygen was provided to the cathode compartment by an air pump through a 0.2 μm filter. The MFC was operated at room temperature (20 ± 2 °C) with magnetic stirring. Each hour, 60 μl of anolyte were collected and analysed with the elaborated sensor.

PAP is degraded, in the anodic chamber by the fungi *T. harzianum*. The degradation generates electrons which flow to the cathodic compartment via the external circuit. Across the membrane, the excess H^+ ions can migrate from the anodic to the cathodic chamber through two mechanisms. The first mechanism involves diffusion, facilitated by water serving as the transporting medium, or acting as a vehicle. The second mechanism occurs via the Grotthuss mechanism, in which the H^+ ions move through the hydrogen bond network of water molecules. In the cathodic compartment, electrons combine with protons that diffuse through the proton exchange membrane and oxygen provided by air to produce water. The flow of electrons from the anode to the cathode generates current and voltage to produce electricity. The internal resistance of the elaborated MFC was 24350 Ω.

Photodegradation set-up and catalyzors elaboration for operation under visible light.—To investigate the applicability of the proposed sensor for the determination of PAP, a residual solution of crystal violet (Cv) degradation from a photoreactor was quantitatively analysed using poly-NiTSPc/Activated-SPE. The experiments have been made in a double-walled borosilicate glass reactor to maintain a constant temperature. This reactor was purchased from SOMIVER, and it processes 500 ml volume. During the manipulation, the reactor was covered with aluminium to reinforce protection and to minimize the penetration of the radiation inside the solution. For the photocatalytic test, we used crystal violet, which is an organic pollutant widely used in textile and pharmaceutical industries. All experiments were carried out in 300 ml of (10 ppm) dye's solution with constant stirring at room temperature using an ultraviolet lamp pencil type UVP furnished by Humeau company, France, with low Mercury vapor pressure in argon for irradiation (25 W, 18 mA) at 254 nm. The $FeVO_4$ which is in our case the

Table I. Preparation of mixed-matrix composite membrane using sulfonated PES with DS of 74% (sPES74) and sulfonated hyper-crosslinked polymer (sHCP).

Membrane composite	sPES (g)	DMC (g)	sHCP (g)	Thickness (μm)	Membrane surface (cm^2)
sPES/sHCPx−0.2	1.00	3.99	0.01	200	1.13

photocatalyst was added to the solution in the dark with continued stirring for 20 min to establish the equilibrium between the solid and the solution and to ensure no adsorption. Subsequently, the photodegradation was started, and launched for 60 min. A small volume of Cv solution was taken at different times and centrifuged for 10 min prior to analysis. The photodegradation of Cv was evaluated by measuring the absorbance at 560 nm.[39]

Results and Discussion

Electrodeposition of poly-NiTSPc film on the activated SPE.— The voltammogram illustrating the process of poly-NiTSPc film deposition on activated SPE is shown in Fig. 1.

In Fig. 1, a redox signal is observed at 0.3 V Ag^{-1} and 0.45 V Ag^{-1} which increases during the scanning. These signals correspond to the electrochemical oxidation and reduction of (Ni^{II}/Ni^{III}).[13,33] The increasing redox signals indicates the electrodeposition of poly-NiTSPc film on SPE. During the electrodeposition, oxo bridges (O-Ni-O) are generated on the SPE surface, these oxo bridges are responsible for the enhancement of the electrocatalytic activity of nickel tetratsulfonated phthalocyanine.[40,41] In order to confirm the presence of the NiTSPc film on the SPE surface, we recorded a cyclic voltammogram of poly-NiTSPc/SPE in NaOH 0.1 M (the insert in Fig. 1 shows the obtained voltammogram). The redox signals obtained at 0.3 V Ag^{-1} and 0.55 V Ag^{-1} on this voltammogram display the presence of nickel on the SPE surface and confirm the formation of NiTSPc film on the SPE surface. By following the methodology previously described by Pontié et al.,[42] the hatched part of the voltammogram allows the determination of the electrode coverage degree and subsequently the deduction of the thickness (e) of the deposited material, calculated to be 39 nm.

EDX characterizations of the elaborated SPEs.—EDX spectra (Fig. 2) show a clear difference between the unmodified SPE and the modified SPEs. The presence of carbon and oxygen is evident on each electrode due to the raw materials used for the fabrication of SPE. In addition to these elements, the spectrum of the activated/SPE shows the presence of sulphur due to the activation of the electrode in sulfuric acid solution. The presence of nickel and sulphur atoms on the poly-NiTSPc/SPE and poly-NiTSPc/activated-SPE spectra demonstrates the effective deposition of poly-NiTSPc film on these electrodes. Also, we note the presence of phosphorus, chlorine and sodium elements likely due to the buffer solution that we used. All these results confirm the successful modification of the SPE surface.

Electrochemical impedance spectroscopy (EIS), real surface area determination and 2D microscopic characterizations.—The electrochemical properties of modified electrodes were investigated using EIS and cyclic voltammogram of $[Fe(CN)_6]^{3-/4-}$ used as a probe. EIS is an accurate tool that allowed us to study charge transfer rates for unmodified and modified SPEs. Figure 3 shows the Nyquist diagrams of the different tested electrodes recorded in the presence of 5 mM $[Fe(CN)_6]^{3-/4-}$ in 0.1 M KCl.

Nyquist diagrams represent the charge transfer resistance at the electrode/electrolyte interface. One can observe in Fig. 3, four semi-circles with different diameters. The charge transfer resistances (Rct) were obtained to be 1085 Ω, 630 Ω, 447 Ω and 254 Ω for unmodified SPE, poly-NiTSPc/SPE, activated/SPE and poly-NiTSPc/activated SPE, respectively. These results firstly confirm those obtained with

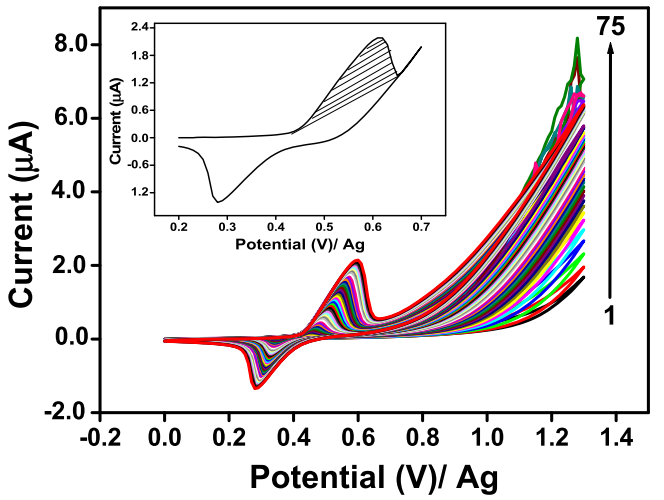

Figure 1. 75 cyclic voltammograms on the activated SPE in the presence of 0.1 M NaOH + 2 mM NiTSPc. Potential scan rate: 100 mV s^{-1}. Insert shows a cyclic voltammogram recorded on poly-NiTSPc/activated SPE in 0.1 M NaOH after the electrodeposition of poly-NiTSPc film.

optical microscopy and EDX spectrum displaying that the modification changes the surface of the electrode and then show that the different modification improves SPE performances. We can observe that the activated SPE is more conductive than the poly-NiTSPc/SPE, while poly-NiTSPc/activated SPE shows a better conductivity. The decrease of Rct which corresponds to the decrease of charge transfer resistance is firstly due to the effect of activation which facilitates electron transfer during the electrochemical reaction and then to the presence of poly-NiTSPc film on the electrode surface, which leads to an enhancement of the electron transfer rate for the $[Fe(CN)_6]^{3-/4-}$ redox system.[19,23] Moreover the CV recorded in 5 mM of $[Fe(CN)_6]^{3-/4-}$ solution using unmodified SPE, poly-NiTSPc/SPE, activated/SPE and poly-NiTSPc/activated SPE (Fig. 4) show a significant reduction of ΔE peak (separation between anodic and cathodic peak) from 280 mV to 140 mV for unmodified SPE, and activated SPE respectively, confirming the role of the activation process on electrocatalytic behavior of the developing sensors. One can also observe an increase of oxidation and reduction peaks of $[Fe(CN)_6]^{3-/4-}$ for each modified electrode with a significant increase of poly-NiTSPc/activated SPE compared to the other electrodes, traducing the good electrocatalytic activity of modified electrodes.

The obtained voltammograms were also helpful in calculating the real surface area of SPEs using the Randles Sevcik formula:

$$Ip = (2.69 \times 10^5) n^{3/2} A D^{1/2} C v^{1/2} \quad [2]$$

Where n is the number of electrons exchanged, A in cm^2 is the active area of the electrode, with $D = 0.62 \times 10^5$ cm^2 s^{-1} is the diffusion coefficient, C in mol cm^{-3} is the concentration of $[Fe(CN)_6]^{3-/4-}$ and v is the potential scan rate.[43] Results are presented in Table II.

We can observe in Table II that the real surface area increases two times from 0.082 cm^2 to 0.167 cm^2 for unmodified SPE and poly-NiTSPc/activated SPE respectively. Poly-NiTSPc/SPE and activated SPE exhibited a real surface area of 0.100 cm^2 and 0.137 cm^2, respectively. The geometric area of the four electrodes

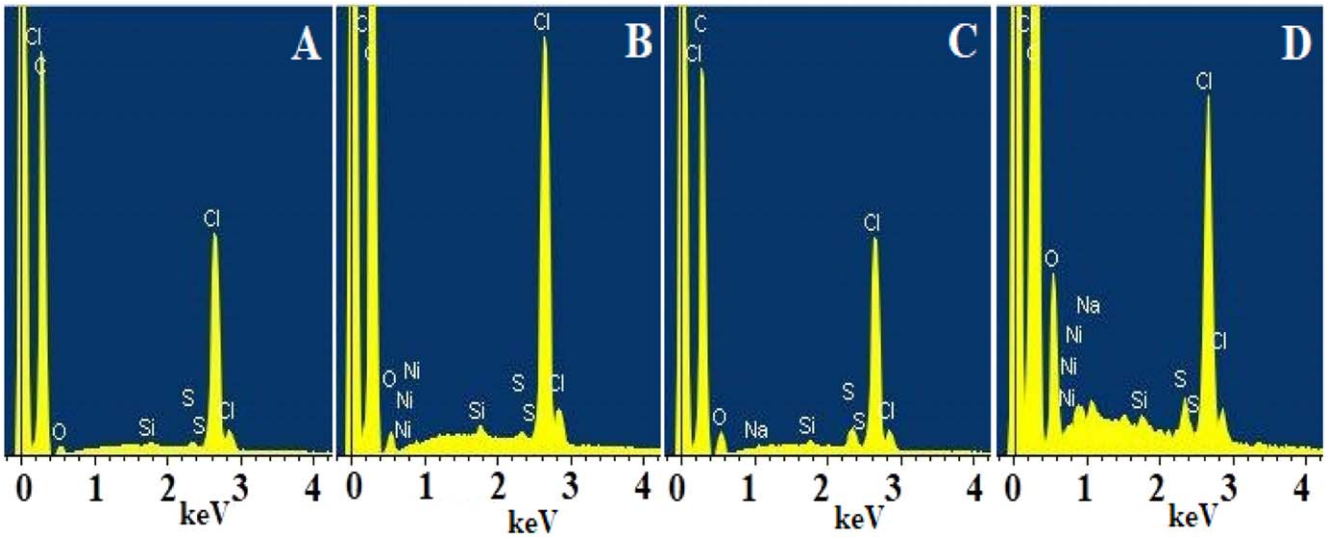

Figure 2. EDX spectra of A-unmodified SPE, B- poly-NiTSPc/ SPE, C- Activated/ SPE and D- poly-NiTSPc/activated SPE.

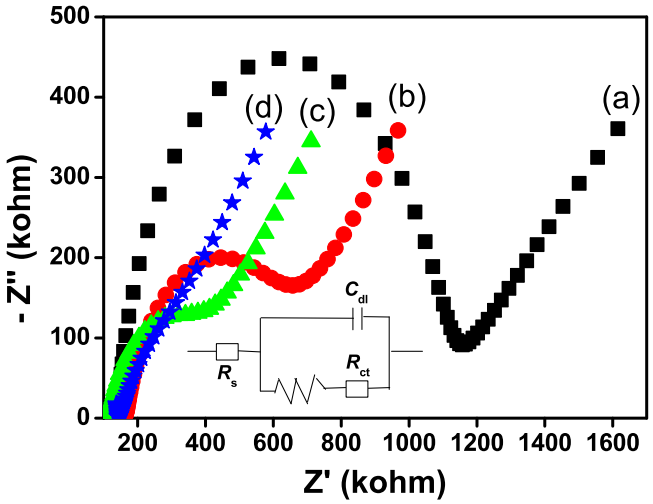

Figure 3. Nyquist plots of (a) unmodified SPE, (b) poly-NiTSPc-SPE (c) Activated/SPE and (d) poly-NiTSPc/Activated-SPE obtained in 5 mM $[Fe(CN)_6]^{3-/4-}$ (1:1) solution containing 0.1 M KCl. The frequency range was from 1 kHz to 10^4 MHz. The Inset shows the corresponding equivalent circuit.

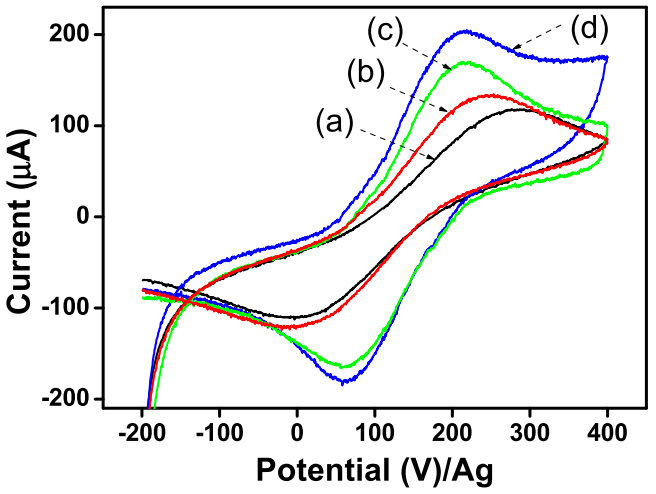

Figure 4. CV of (a) unmodified SPE, (b) poly-NiTSPc-SPE (c) Activated-SPE and (d) poly-NiTSPc/Activated-SPE obtained in 5 mM $[Fe(CN)_6]^{3-/4-}$ (1:1) solution containing 0.1 M KCl, v = 0.1 V.s^{-1}.

was 0.126 cm^2 for each calculated using the formula $S = \pi r^2$ with r = 0.20 cm. It appears that the geometric is greater than the active surface area. Same results were observed by Deffo et al. [44] This result is likely due to the fact that not all of the geometric area is electrochemically active. The greatest active surface area with 0.167 cm^2 was obtained for poly-NiTSPc/activated SPE justifying its higher sensitivity in comparison to SPEs.

The 2D microscopy characterization aided the determination of the roughness of the different SPEs and the obtained values of roughness are shown in Table II. The unmodified SPE shows an average roughness of 11.6 μm while poly-NiTSPc/SPE, activated/ SPE and poly-NiTSPc/activated SPE exhibit an average roughness of 7.6, 4.2 and 3.1 μm, respectively. These results demonstrate that the combination of activation and poly-NiTSPc film enhances the surface of the electrode leading to an increase in the conductivity.

Electrochemical determination of PAP on the elaborated sensors using CV and DPV.—CV and DPV were used to evaluate the electroactivity of PAP and to observe the effect of SPEs modification on PAP peak. For this purpose, CV and DPV curves were recorded with 5 mg l^{-1} of PAP in ABS (0.1 M pH = 5). Figure 5 shows the obtained voltammograms.

As seen in Fig. 5, the cyclic voltammetry shows a reversible signal of PAP with an anodic peak appearing at Epa = 0.05 V Ag^{-1} and a reduction peak at Epc = 0.02 V Ag^{-1} corresponding to the following redox equation.[19]

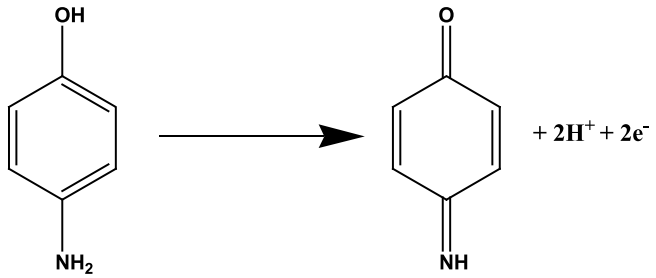

Equation 1: Half redox reaction of PAP direct oxidation

The electrochemical direct oxidation reaction of PAP results in 4-quinoneimine with the release of $2H^+$ and $2e^-$.[45] In Fig. 5A, a decrease in the separation of anodic and cathodic peak potential (ΔE peak) for each modified SPE compared to the unmodified SPE is

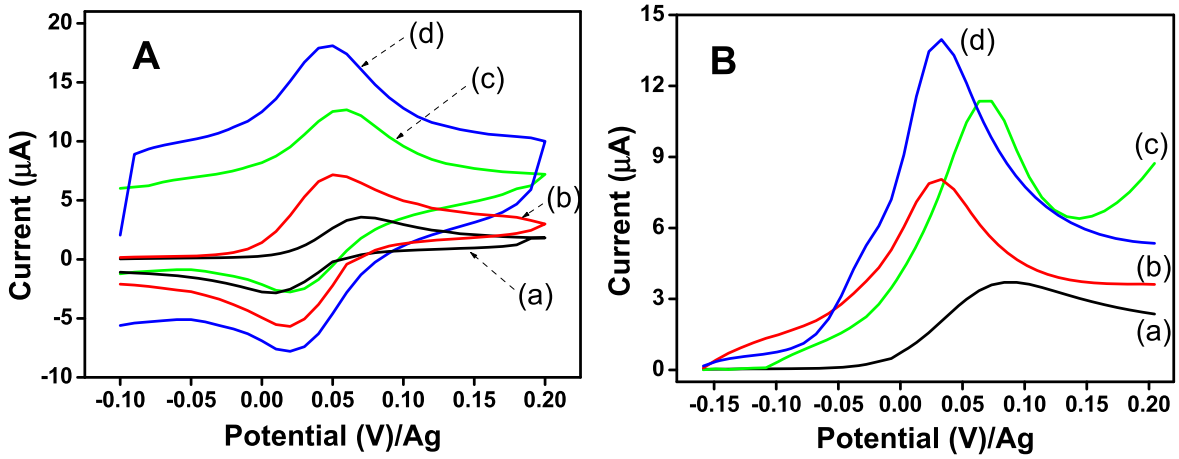

Figure 5. A- CV and B- DPV of 5 mg l^{-1} of PAP in 0.1 M ABS (pH 5) on (a) unmodified SPE, (b) poly-NiTSPc/SPE (c) Activated SPE and (d) poly-NiTSPc/Activated SPE. Potential scan rate 100 mV s^{-1}. DPV parameters were: step potential 5 mV, pulse potential 50 mV, and pulse time 20 ms.

Table II. Active surface area, resistance of charge transfer and roughness of the different elaborated electrodes.

Electrodes Parameters	Unmodified SPE	poly-NiTSPc/SPE	Activated SPE	poly-NiTSPc/Activated SPE
Geometric area (cm^2)	0.126	0.126	0.126	0.126
Active surface area (cm^2)	0.082	0.100	0.137	0.167
Resistance of charge transfer (Ω)	1085	630	447	254
Roughness (μm) (×100)	11.6	7.6	4.2	3.1

observed. In fact, the ΔE peak of PAP is 20 mV for both poly-NiTSPc/SPE and poly-NiTSPc/activated SPE which is lower than that of activated-SPE (35 mV) and unmodified SPE (55 mV). This result confirms that poly-NiTSPc/activated SPE exhibits a better electron transfer rate. Then, both DPV and CV reveal an increase in PAP peak intensity. In DPV, PAP peak intensity for poly-NiTSPc/SPE and activated SPE is twofold and fourfold higher respectively compared to the unmodified SPE. Poly-NiTSPc/activated SPE showed a superior result with a 4.5-fold higher peak confirming its more conductive surface and enhanced electrocatalytic behavior toward PAP analysis.

Calibration curves and detection limits of PAP on the elaborated SPEs in DPV.—Under optimized experimental parameters step potential 5 mV, pulse potential 50 mV and pulse time 20 ms (results not shown), DPV was used to establish the effect of PAP concentration at the proposed modified electrode. For this purpose, increasing concentrations of PAP were consecutively added to the SPEs surface and the corresponding voltammograms were recorded. Figure 6 shows the obtained results.

As expected, Fig. 6 shows an increase of the PAP oxidation peak with the increasing concentration of PAP (0.1 mg l^{-1} to 2.4 mg l^{-1}) for each electrode. Figure 6E exhibits an excellent relationship between the anodic peak and the concentration with a high correlation coefficient of 0.99 for each SPE. The relation between concentration and the peak intensity is given by $Ip_{(a)} = 2.02*[PAP]–0.12$; $Ip_{(b)} = 4.39*[PAP] + 0.14$; $Ip_{(c)} = 5.10*[PAP] + 0.20$ and $Ip_{(d)} = 5.61*[PAP] + 0.28$, respectively for unmodified SPE, poly-NiTSPc/SPE, activated/SPE and poly-NiTSPc/activated SPE. Based on signal to noise ratio of 3.33, these results allowed us to estimate LOD of 74 μg l^{-1} (0.67 μM), 34 μg l^{-1} (0.31 μM), 29 μg l^{-1} (0.29 μM), 26 μg l^{-1} (0.23 μM) respectively, for unmodified SPE, poly-NiTSPc/SPE, activated/SPE and poly-NiTSPc/activated SPE. The LOQ were also evaluated based on signal to noise ratio of 10 and we obtained 247 μg l^{-1}, 113 μg l^{-1}, 98 μg l^{-1} and 89 μg l^{-1}, respectively for unmodified SPE, poly-NiTSPc/SPE, activated/SPE and poly-NiTSPc/activated SPE. Based on all these results, poly-NiTSPc/activated SPE was selected among unmodified SPE, poly-NiTSPc SPE, and activated SPE as the best electrocatalytic material for PAP detection.

Table III summarizes the analytical performances of other modified electrodes for PAP analysis.

Data from Table III show that both the linear range and limit of detection displayed by the proposed sensor are better than most of those that have been reported demonstrating a great sensitivity of the present sensor. However, our sensor is outperformed by the sensors described in the Ref. 51. Future studies will investigate the combination of nanoparticles (gold and/or nickel) with poly-NiTSPc film for a better sensitivity of the proposed sensor.

Reproducibility, repeatability and stability.—Experiments were carried out to evaluate the reproducibility, repeatability and the stability of the proposed sensor and Fig. 7 shows the obtained results. The reproducibility of poly-NiTSPc/activated SPE Fig. 7A was investigated by recording DPV measurement in 0.1 M ABS containing 1 mg l^{-1} of PAP using five different poly-NiTSPc/activated SPE fabricated individually using the same protocol.[52] The relative standard deviation RSD was found to be 3.9% indicating that the developed sensor has good reproducibility. The repeatability of the sensor was evaluated by repeating the measurement for five days in an ABS sample containing the same concentration of PAP and using the same poly-NiTSPc/activated SPE (SPE 3) Fig. 7B. The obtained RSD value was 5.3% for the peak current measured, which also demonstrated the repeatability of the proposed sensor.

After around twenty analyses carried out in a microbial fuel cell dedicated to the bioremediation of PAP, the stability of the proposed sensor was evaluated by comparing $[Fe(CN)_6]^{3-/4-}$ (5 mM) current peak before and after the series of analysis Fig. 7C. We observed a slight decrease of the oxidation peak current of $[Fe(CN)_6]^{3-/4-}$ evaluated to be 3.84%. Furthermore, a decrease in ΔE_{peak} (=Epa −Epc) from 0.21 V Ag^{-1} to 0.19 V Ag^{-1} was observed in Fig. 7C.

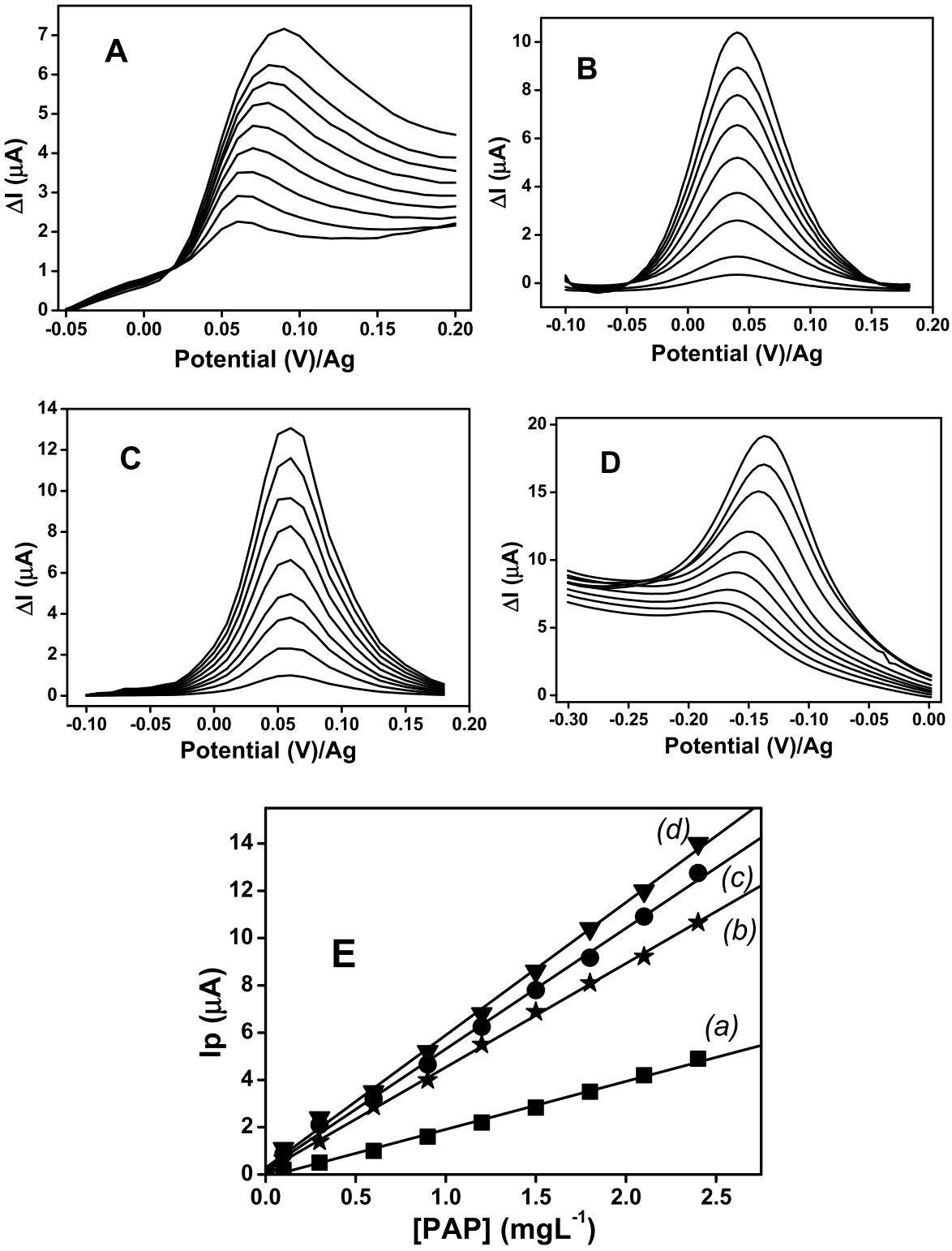

Figure 6. DPV on A- unmodified SPE, B- poly-NiTSPc/SPE C- Activated/SPE and D- poly-NiTSPc/Activated-SPE in 0.1 M ABS (pH 5) at different concentrations of PAP: 0.1, 0.3, 0.6, 0.9, 1.2, 1.5, 1.8, 2.1 and 2.4 mg l^{-1}. E- shows the corresponding calibration curves.

The drop in signal intensity corresponds to a reduction of surface area from 0.044 cm^2 to 0.042 cm^2. These results indicate that the proposed sensor is reasonable stable and can be used for multiple consecutive PAP measurements.

All measurements carried out in the microbial biofuel cell with the tested SPE are reported in Application of poly-NiTSPc/activated SPE for PAP biodegradation study in the MFC section.

Application of poly-NiTSPc/activated SPE for PAP biodegradation study in the MFC

IC_{50} of T. harzianum in presence of PAP.—IC_{50} is the concentration of pollutant necessary to inhibit 50% of the fungi growth. It is a key parameter of the experiment that aids the selection of the appropriate concentration of PAP for the experiments in MFC. The

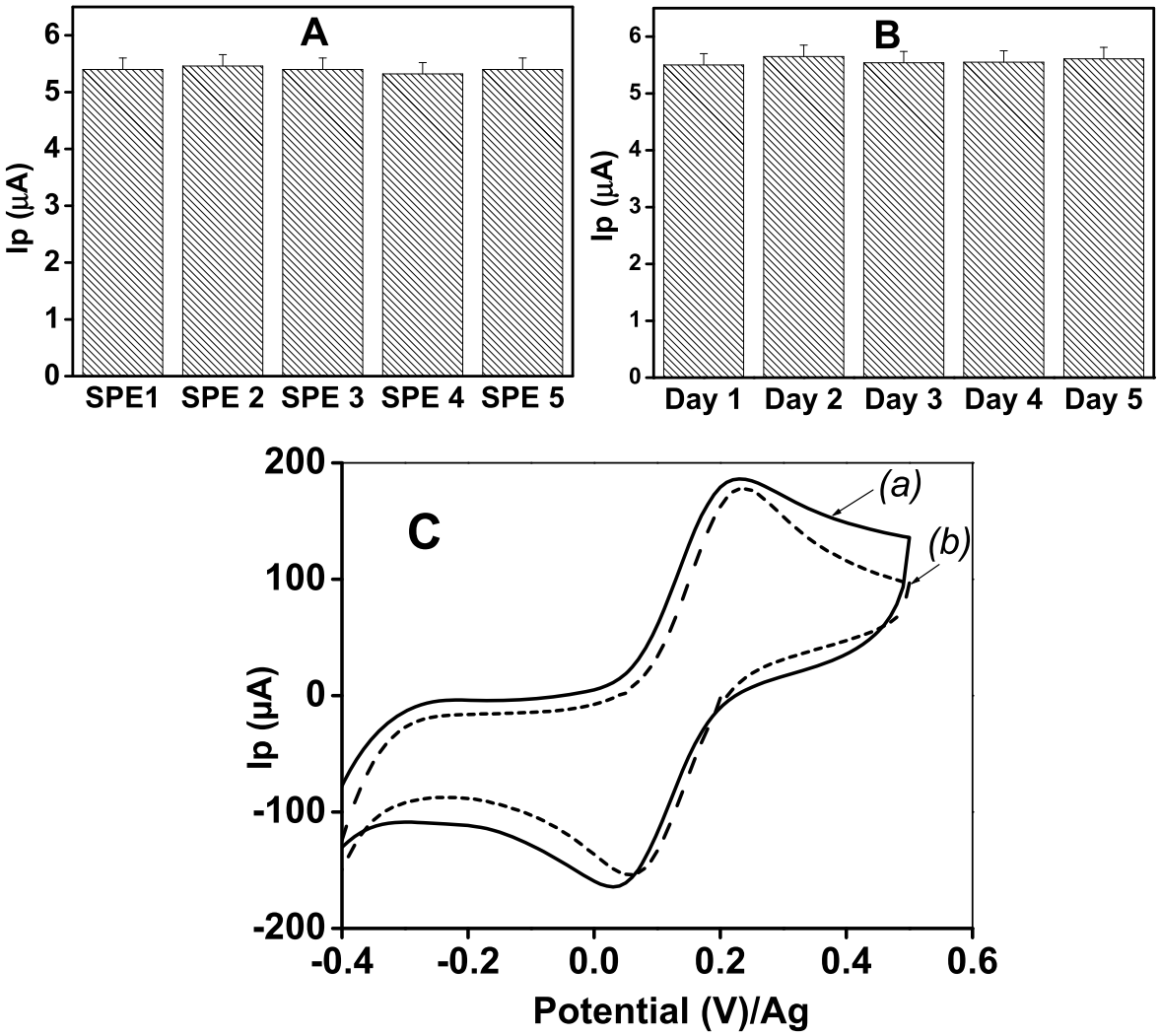

Figure 7. A reproducibility histogram of 5 tested SPE, B repeatability histogram for the tested SPE 3 in 1 mg l^{-1} of PAP in ABS pH = 5, 0.1 M; C Shows the durability data using CV occurred in 5 mM of $[Fe(CN)_6]^{3-/4-}$ recorded before (a) and after (b) 2 campaigns of PAP bioremediation studies conducted in MFC (20 measurements of samples taken in the MFC).

Table III. Comparison of detection limits of different modified electrodes and the sensor used in this work.

Electrodes	pH	Method	Sensitivity (μA/μM)	Linear range (μM)	LOD (μM)	References
Ag/CPE[a)]	6.0	SWV	0.61	9.1–100.7	0.38	9
bis-Shiff-Co/GCE[b)]	7.0	DPV	25	5−30	2.08	46
S-CTFs@$NiCo_2O_4$/GCE[c)]	6.0	DPV	0.0654	2–360	0.35	47
NiNPs-SDS/CS/SPE[d)]	7.0	DPV	0.959	0.5–350	0.06	48
AuNPs/CNTs-CONH-TAPP/GCE[e)]	7.0	DPV	0.320	0.08–60	0.44	49
Hemin-graphen/GCE[f]	7.0	DPV	31.02	0.3–25	0.06	50
ZnO/NPC/GCE[g)]	7.4	DPV	0.411	5−120	0.014	51
Unmodified SPE	7.2	DPV	0.22	0.9–21	0.67	This work
poly-NiTSPc-SPE	7.2	DPV	0.48	0.9–21	0.31	This work
Activated-SPE	7.2	DPV	0.56	0.9–21	0.29	This work
poly-NiTSPc/Activated-SPE	7.2	DPV	0.62	0.9–21	0.23	This work

a) Carbon paste electrode modified with Arabic gum b) bis-Schiff base cobalt complex modified Glassy carbon electrode (GCE) c) S-CTFs: Sulfurbridged covalent triazine frameworks; $NiCo_2O_4$: Nickel cobaltite d) Chitosan coated Nickel Nanoparticles onto Screen Printed Electrode (SPE) e) AuNPs gold nanoparticles; CONH-TAPP Tetraaminophenyl porphyrin functionalized multi-walled carbon nanotube g) NPC: Nanoporous carbone

aim is to understand the inhibition effect of PAP on *T harzianum* growth, which was studied on PGA plates with PAP concentrations ranging from 10 and 1000 mg l^{-1}. Figure 8 shows the growth of *T. harzianum* at different concentrations of PAP.

We can distinguish two main parts for each curve in Fig. 8. The first part (0 to 12 h) shows a slow growth of the fungi known as the latency phase and the second part (beyond 12 h) shows a rapid growth of the fungi called exponential growth. We determined the

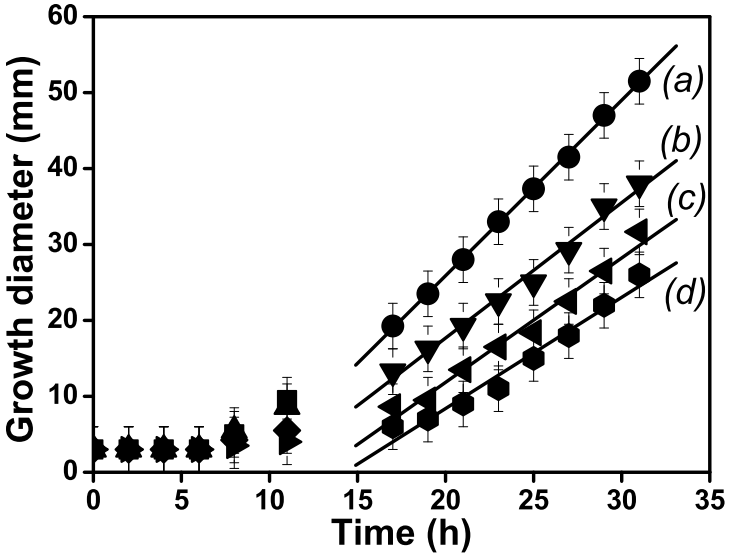

Figure 8. *T. harzianum* growth curves in the presence of increasing PAP concentration C_{PAP} 0 mg l^{-1} i.e. control (a); 100 mg l^{-1} (b); 500 mg l^{-1} (c);1000 g l^{-1} (d).

slope values during the exponential phase for each curve. The percentage of inhibition was then calculated using the following formula.[28]

$$Inhibition\,(\%) = \frac{Slope\ control - Slope\ Cpap}{Slope\ control} \times 100 \qquad [3]$$

Table IV presents the slope of each curve from Fig. 8.

Figure 9 shows the percentage of inhibition vs PAP concentration.

In Fig. 9, the percentage of inhibition of the fungi increases as the PAP concentration increases. With 100 mg l^{-1} of PAP, we have only 6% of *T harzianum* inhibition. Significant inhibition of the fungi is observed beyond 200 mg l^{-1}. The IC_{50} for PAP toward *T harzianum* was 900 mg l^{-1}. Our application focused on hospitals and industries effluent where PAP concentrations encountered are very high. Based on this and the IC_{50} value, we decided to perform our study in the MFC with 100 mg l^{-1} of PAP to investigate the treatment of pollutants in real media.

Morphological characterization of the bioanode.—Figure 10 shows the SEM images obtained on carbon cloth before and after colonization with the fungi *T. harzianum*.

We note a distinct difference between the unmodified (Fig. 10A) and modified CC (Fig. 10B). Figure 10C shows the carbon cloth covered with the fungi at a magnification of ×100. Figure 10B revealed a remarkable and convincing pure biofilm formation composed of filamentous fungi attesting to the presence of the fungi on the CC. SEM images provide valuable visual information on the fungi morphology; mycelium including filament thickness was evaluated to be 2.5 μm and the spore diameter was 2 μm. We also note that the biofilm has largely covered the CC indicating the good fixation of the fungi *T. harzianum* on the carbon cloth.

Characterization of the elaborated membrane.—The CEC of the elaborated membrane was calculated to be 0.6 mEq.g^{-1} showing a good cation conductivity due to the sulfonate group.[38] This value is acceptable for our bioremediation study and this type of novel membrane has been validated in another study.[29] However, this value is lower than the CEC of classic Nafion membrane (0.86 mEq g^{-1}).[29]

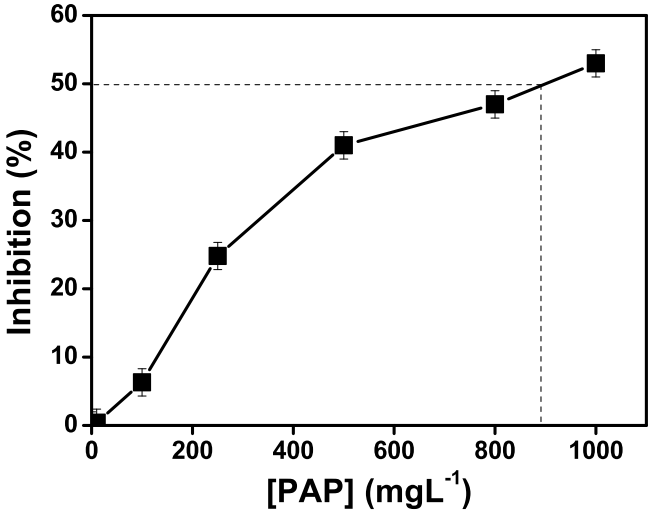

Figure 9. *T. harzianum* inhibition rate at different PAP concentrations.

Polarization curves to set MFC flowing conditions.—Polarization curves are useful to understand the relationship between voltage, current and power in the MFC system. This can also provide insights to determine an optimal resistance allowing the MFC to flow in the best conditions. Polarization curves were obtained by varying the external resistance (R in Ω) from 10 MΩ to 1 kΩ and recording the resulting electromotive force FEM (E in V). The Open circuit potential is determined when the external resistance is fixed at 10 MΩ. Current intensity (I in A) is calculated using Ohm's law given by the following formula:

$$E = R.I \qquad [3a]$$

Table IV. Slope and inhibition percentage of the graph of growth diameter vs time.

PAP concentration (mg l^{-1})	0 (Control)	10	100	250	500	800	1000
Slope (mm h^{-1})	2.245	2.23	2.07	1.66	1.30	1.16	1.06
Inhibition (%)	0	0.4	6.3	24.8	41	47	53

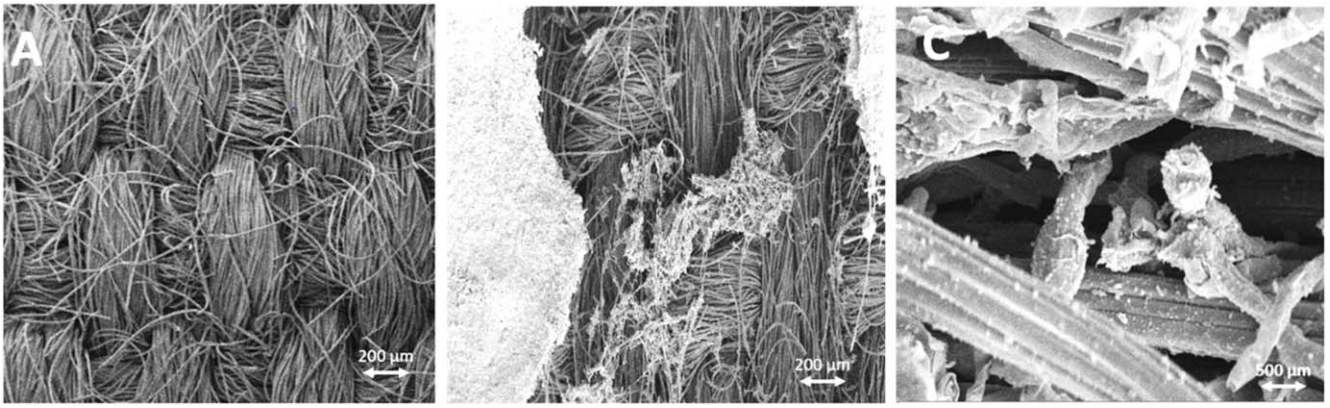

Figure 10. SEM images of (A) unmodified Carbon cloth, (B) and (C) Carbon cloth covered by *T. harzianum* mycelium.

The power output was determined as follows

$$P = R.I^2 \quad [4]$$

Figure 11 shows the plot of EMF and power density vs current density (j).

From Fig. 11, we can see that the open circuit potential (OCP), which corresponds to the value of EMF when the current density is 0 was found to be 365 mV. The slope of E = f(j) at the beginning of the experiment is 7727 Ω, which constitutes the optimal resistance of the MFC. The MFC was set up at this value for better flow. Moreover, the representation of P as a function of j shows a parabola according to the Eq. 3. The maximum power is obtained at the maximum of the parabola. The obtained Pmax is 95 mW m^{-3}.

Calibration curve of poly-NiTSPc/activated SPE for PAP biorremediation monitoring.—To determine the PAP residual concentration in the MFC over time, we carried out a calibration curve that links the peak intensity to the analyte concentration. DPV was performed under optimized operating conditions using poly-NiTSPc/activated SPE in ABS (0.1 M pH = 5) in the PAP concentration range of 10 mg l^{-1} to 100 mg l^{-1}. The obtained voltammograms are illustrated in Fig. 12

The peak observed at 0.13 V Ag^{-1} (Fig. 12) corresponds to the direct oxidation of PAP to 4-quinoneimine as mentioned (Eq. 1). It appears that the oxidation peak intensity increases linearly with the concentration of PAP (insert of Fig. 12). The plot of peak intensity as a function of PAP concentration is expressed by the regression equation Ip(µA) = 1.44[PAP] (mg l^{-1})–6.16.

PAP biodegradation in MFC.—The biodegradation of PAP in the MFC was monitored using the elaborated poly-NiTSPc/activated SPE. At every 1 h, 60 µl of the anolyte is placed on the electrode and analysed using the DPV technique. Figure 13A shows the DPVs of the anolyte solution obtained every hour, while Fig. 13B gives the evolution of PAP concentration over time.

From Figs. 13A and 13B, we observe a gradual decrease in the peak intensity of PAP due to a cleavage of aromatic rings leading to the degradation of the molecule. The fungus appears to use PAP as a source of carbon. The degradation of the molecule is probably due to the action of enzyme laccase known to mineralize organic compounds.[23,29] Additionally, Fig. 13B indicates that the initial PAP concentration in the MFC is 80 mg l^{-1} which is lower than the 100 mg l^{-1} initially introduced. This discrepancy is likely due to the sorption of PAP by the carbon cloth as reported elsewhere on this KIP carbon electrode CC.[28] The nonlinear variation of concentration vs time shown in Fig. 13B suggests that the degradation of the pollutant in the MFC does not obey 0-order kinetics. To explicate our results, we then modelled the degradation kinetics by plotting ln(C/C_0) vs time displayed in Fig. 14.

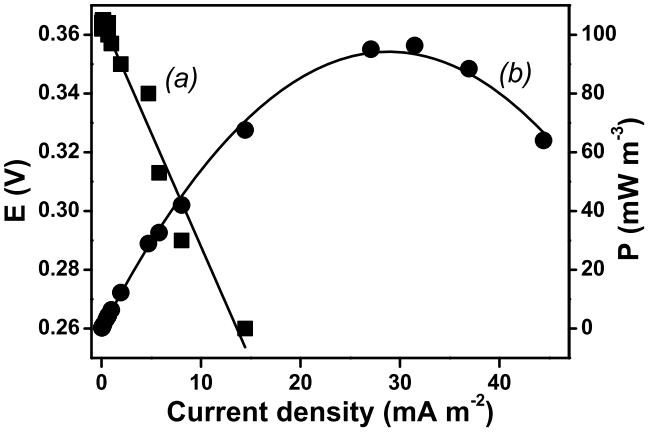

Figure 11. Polarization curves for PAP biodegradation in the MFC: (a) potential vs current density and (b) Power density vs current density.

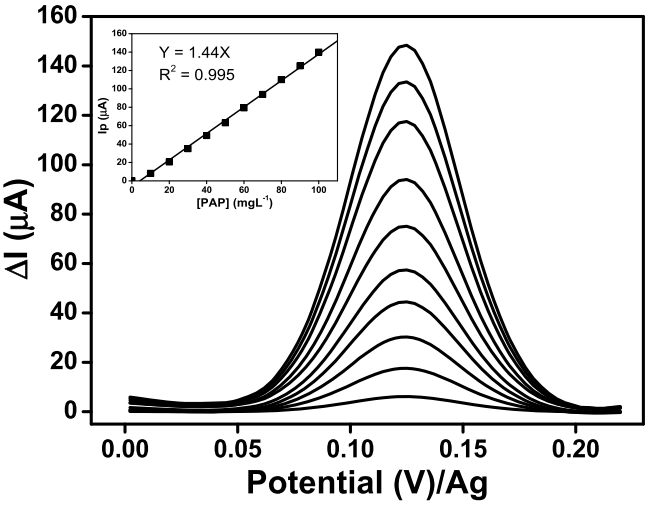

Figure 12. DPV on poly-NiTSPc/activated SPE in 0.1 M ABS (pH 5) at different concentrations of PAP 10; 20; 30; 40. 50; 60; 70; 80; 90 and 100 mg l^{-1}. Insert shows the peak currents vs PAP concentrations. DPV parameters were: step potential 5 mV, pulse potential 50 mV, and pulse time 20 ms.

This plot displays a linear variation of ln(C/C_0) = f(t) indicating that the degradation in the MFC follows a first-order kinetic with a kinetic constant of 0,063 h^{-1} and a half-life time of 11 h. The half-life time is calculated using $t_{1/2} = \ln 2/k$ (where k is the kinetic

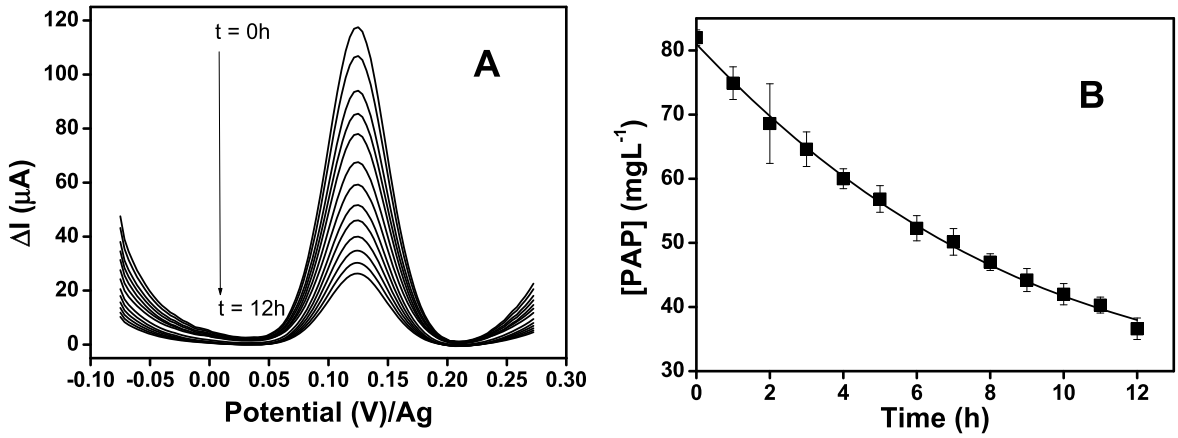

Figure 13. A- DPVs of anolyte solution over time, (B) Evolution of PAP concentration over time. DPV parameters were: step potential 5 mV, pulse potential 50 mV, and pulse time 20 ms.

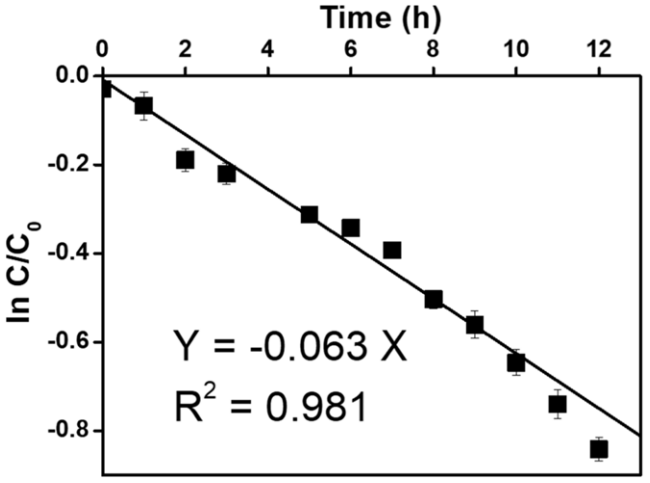

Figure 14. Biodegradation kinetic of PAP by the biofilm of *T. harzianum* over time.

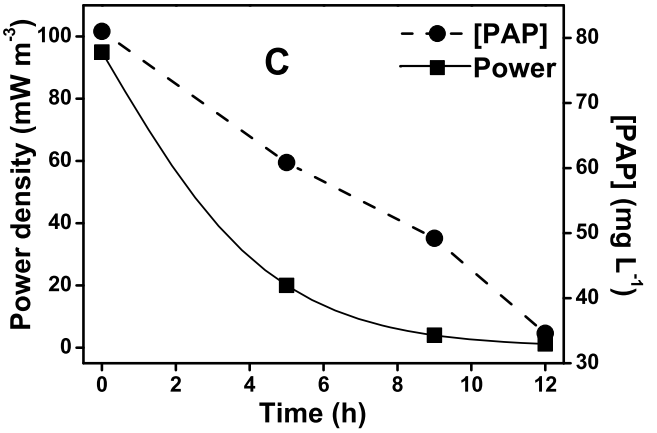

Figure 15. PAP concentration vs time in the MFC and MFC power density vs time.

constant). Furthermore, in Fig. 15 a strong correlation between PAP degradation in MFC and power density is evident which decreases over time from 95 mW m^{-3} to 1.2 mW m^{-3}.

When PAP concentration is high in the MFC, many electrons are produced during its degradation, resulting in higher power output. As the PAP concentration decreases fewer electrons are produced thus the lower the MFC power density.

Table V compares the biodegradation kinetic rate for two ascomycota species, *Scedosporium dehoogii* and *T. harzianum* MFC studies.

In Table IV we observe that the fungus (*T. harzianum*) used in the present study shows a faster degradation rate than the MFC working with *Scedosporium dehoogii.*

Assuming the fungi's ability to completely mineralize PAP, we can suggest potential reactions that could occur in MFC.

$$C_6H_7NO + 11H_2O \rightarrow 1/2N_2 + 6CO_2 + 29H^+ + 29e^-$$

$$29/4\ O_2 + 29\ H^+ + 29\ e^- \rightarrow 29/2\ H_2O$$

$$C_6H_7NO + 29/4\ O_2 \rightarrow 1/2\ N_2 + 6\ CO_2 + 7/2\ H_2O$$

29 mol of electron are produced per mol of PAP compared to 24 mol of electron per mol of glucose as usually known.

Applicability of poly-NiTSPc/activated SPE for the illustration of PAP formation during the photodegradation of crystal violet.— Crystal violet (Cv) is a triphenylmethane dye widely used in textile and ink industries for dyeing and printing.[54] Despite its numerous uses Cv poses a significant risk for both humans and the environment. It is well known that Cv is persistent in the environment for long periods.[55] As a result, researchers have studied the biodegradation of Cv using different approaches. *Votat* et al. investigated the biodegradation of Cv using a *Trichoderma harzianum* microbial fuel cell achieving a 55% degradation of Cv after 40 h.[28] To enhance Cv degradation, we propose an advanced oxidation process (photodegradation) of Cv 3 mg l^{-1} using Ag $FeVO_4$ 0.5 g l^{-1} as photocatalyst to applied photocatalysis method. The concentration of Cv over time was tracked using a spectrophotometer. Figure 16A shows the obtained results.

Figure 16A shows a gradual decrease of the Cv concentration over time which can be attributed to its degradation into the photoreactor. The photodegradation system achieved significant efficiency after 60 min. At the end of the process, the solution becomes clear with a Cv degradation rate of 96.5%. The Cv degradation kinetic was modelled by plotting $\ln(C/C_0)$ vs time (Fig. 16C). This plot shows a linear variation indicating that a first order kinetic degradation occurred with a constant rate of 0.051 h^{-1} and a half degradation time of 14 min. The mechanism of Cv degradation is shown in Eq. 2.

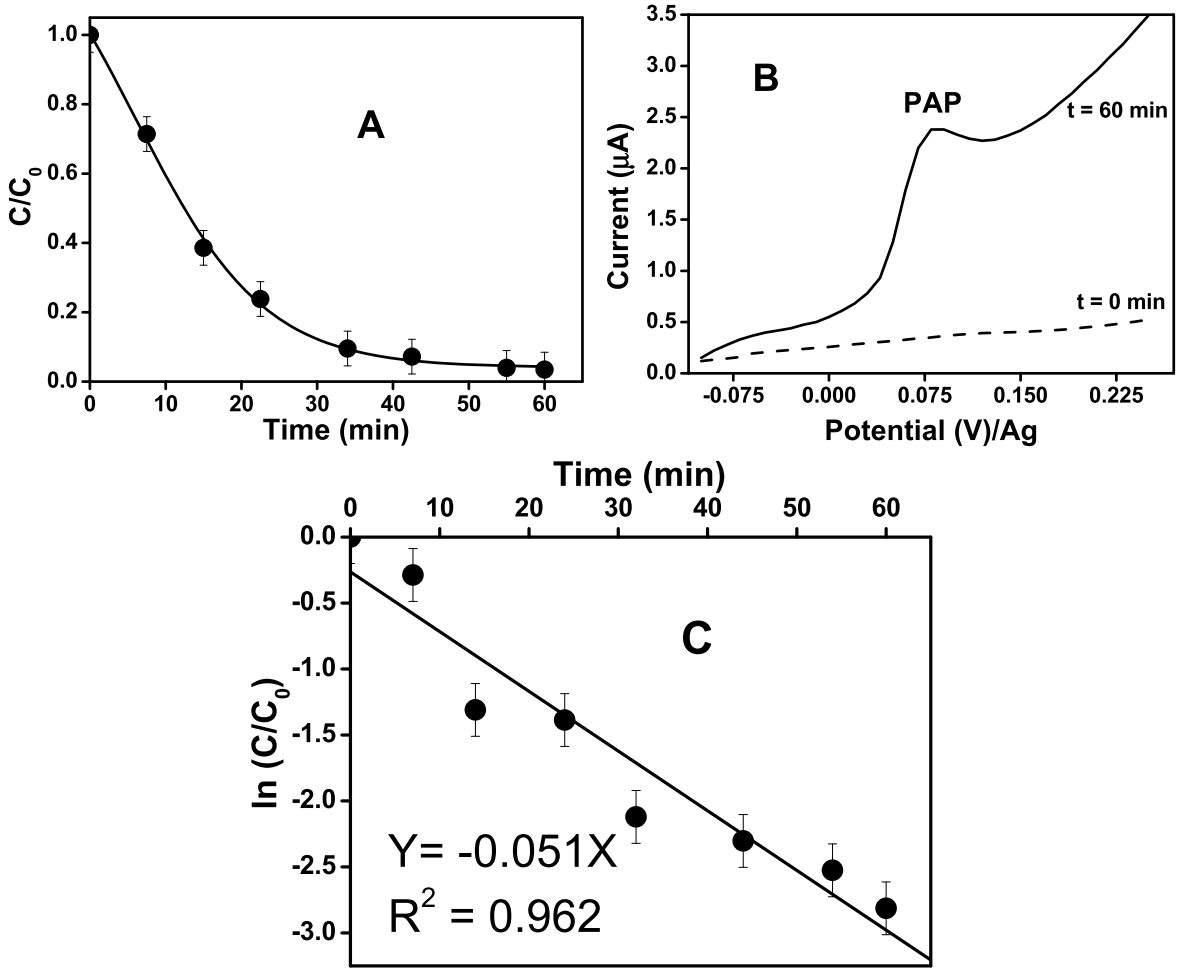

Figure 16. A-Relation of C/C_0 over time. B- DPVs of the residual solution of crystal violet before (t = 0 min) and after (t = 60 min) photodegradation under the following conditions: [Cv] = 3 mg l^{-1}, $V_{solution}$ = 500 ml, pH = 3 and 25 W UV_{254} nm irradiation C-Relation of $\ln(C/C_0)$ as a function of time. DPV parameters were: step potential 5 mV, pulse potential 50 mV, and pulse time 20 ms.

Table V. Comparison between the kinetic rates of biodegradation of various bioanodes in previous studies vs this work.

Pollutant	Bioanode	Constant rate k (h^{-1})	References
PAP	*Scedosporium dehoogii*	0.008	53
Acetaminophen	*Scedosporium dehoogii*	0.046	33
Acetaminophen	*Trichoderma harzianum*	0.095	29
PAP	*Trichoderma harzianum*	0.063	This work

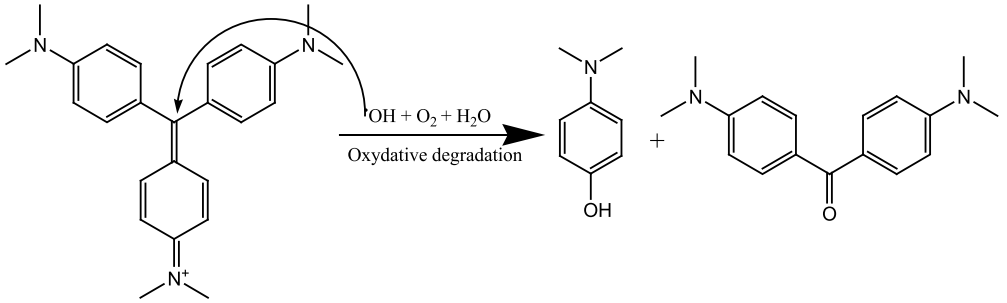

Equation 2: Mechanism of Cv photodegradation with PAP formation as a by-product[56]

The light energy in the form of photons hits the surface semiconductor with energy equal to or higher than the band gap energy of the photocatalyst, the transferred electrons are excited from the valence band to the conduction band, creating hole h^+ in the valence band, after that free radicals are generated, and the oxidation and reduction reactions occur. The holes at the valance band can react with water molecules, to generate hydroxyl radicals, which have a strong oxidizing capability that is used to degrade organic matter. However, electrons at the conduction band can interact with oxygen-generating superoxide anion, this mechanism leads to the formation of new molecules. As PAP is the main degradation by-product of Cv,[56] poly-NiTSPc/activated SPE was applied to analyse the residual solution of Cv after photodegradation and the Fig. 16B shows the obtained results. One can observe a peak at 0.4 V Ag^{-1} attributed to PAP oxidation. This result confirms the partial degradation of Cv with the formation of PAP quantified with the poly-NiTSPc/activated SPE sensor at 300 $\mu g\ l^{-1}$.[57]

Conclusion and Perspectives

A sensitive electrochemical sensor poly-NiTSPc/activated SPE type was developed and applied for PAP analysis in MFC bioremediation study and in a photoreactor after Cv degradation. The MFC results showed that *T. harzianum* fungus exhibited good performance expressed by rapid growth leading to a total mineralization of PAP. The biodegradation process obeyed first-order kinetics with a constant rate of 0.063 h^{-1} and a half degradation time of 11 h. The analysis of the residual solution resulting from the photodegradation of Cv using the developed SPE revealed the presence of PAP as a by-product of this dye. This study also suggests the prospect of bioremediation of organic compounds after the initial photodegradation quick step to produce green bioenergy.

Future investigations will combine both processes (photodegradation first and MFC to achieve the treatment) with the aim of total removal of Cv and their by-products.

Acknowledgments

The authors express their gratitude to the French embassy in Ouagadougou for granting Mr Silga with SCAC scholarship to support his research stay in France. We also thank iMERMAID European research program (*Innovative Solutions for Mediterranean Ecosystem Remediation* via *Monitoring and Decontamination from Chemical Pollutant, EU project number 101112824, iMERMAID.eu*) for supporting J.P. Silga's PhD work. We acknowledge Romain Mallet from the microscopy center of Angers University (SCIAM, France) for recording SEM images and EDX spectra. Many thanks to Henry I. F. Adenusi, an English speaker, for revising the final version of the manuscript. Conflict of interest: The authors declare no competing interests.

ORCID

Pontié Maxime https://orcid.org/0000-0001-8751-3041

References

1. J. C. De Souza, B. F. Da Silva, D. A. Morales, G. D. A. Umbuzeiro, and M. V. B. Zanoni, *J. Hazard. Mater.*, **387**, 122000 (2020).
2. H. Filik et al., *Talanta*, **77**, 103 (2008).
3. S. A. Boltia, A. T. Soudi, E. S. Elzanfaly, and H. E. Zaazaa, *J. Chromatogr. Sci.*, **58**, 223 (2020).
4. N. Hamad Al-Shaalan, I. Ali, Z. A. ALOthman, L. H. Al-Wahaibi, and H. Alabdulmonem, *Molecules*, **24**, 3443 (2019).
5. B. Giri, *in Laboratory Methods in Microfluidics* (Elsevier, Amsterdam)97 (2017).
6. M. S. Mustafa et al., *RSC Adv.*, **14**, 16045 (2024).
7. H. Mahmoudi Moghaddam, H. Beitollahi, S. Tajik, I. Sheikhshoaie, and P. Biparva, *Environ. Monit. Assess.*, **187**, 407 (2015).
8. L. Y. Shiroma, M. Santhiago, A. L. Gobbi, and L. T. Kubota, *Anal. Chim. Acta*, **725**, 44 (2012).
9. S. M. Foukmeniok et al., *J. Appl. Electrochem.*, **49**, 575 (2019).
10. M. Pontie et al., *J. Appl. Electrochem.*, **53**, 1701 (2023).
11. B. Ouedraogo, S. Baachaoui, A. Tall, I. Tapsoba, and N. Raouafi, *Microchim. Acta*, **190**, 316 (2023).
12. S. Tajik, H. Beitollahi, S. Shahsavari, and F. G. Nejad, *Chemosphere*, **291**, 132736 (2022).
13. H. Beitollahi, S. Tajik, H. K. Maleh, and R. Hosseinzadeh, *Appl. Organomet. Chem.*, **27**, 444 (2013).
14. C. Gibi, C-H. Liu, S. C. Barton, S. Anandan, and J. J. Wu, *J. Taiwan Inst. Chem. Eng.*, **154**, 105071 (2024).
15. S. Tajik, M. A. Taher, and H. Beitollahi, *J. Electroanal. Chem.*, **720–721**, 134 (2014).
16. H. M. Moghaddam et al., *Russ. J. Electrochem.*, **53**, 452 (2017).
17. G. Liang et al., *Environ. Technol. Innov.*, **28**, 102922 (2022).
18. H. Mahmoudi-Moghaddam, S. Tajik, and H. Beitollahi, *Food Chem.*, **286**, 191 (2019).
19. S. M. Foukmeniok et al., (2022), J.-J. Feng, Editor.*Int. J. Anal. Chem.*, **2022**, 1.
20. H. H. Tchoumi Bougna et al., *J. Appl. Electrochem.*, **54**, 2121 (2024).
21. Y. F. R. Bako, S. F. Mbokou, B. Kaboré, I. Tapsoba, and M. Pontié, *Mater. Sci. Appl.*, **15**, 25–35 (2024).
22. P. A. Raymundo-Pereira, N. O. Gomes, S. A. S. Machado, and O. N. Oliveira, *J. Electroanal. Chem.*, **848**, 113319 (2019).
23. Y. F. R. Bako, J-P. T. Silga, S. Mbokou Foukmeniok, M. Pontié, and I. Tapsoba, *J. Appl. Electrochem.*, **54**, 1253 (2024).
24. Sabreena et al., *Plants*, **11**, 1255 (2022).
25. C. Ratiu et al., *Chem. Pap.*, **65**, 23 (2011).
26. B. B. Tewari, *Russ. J. Phys. Chem. A*, **88**, 1564 (2014).
27. H. Claus, G. Faber, and H. König, *Appl. Microbiol. Biotechnol.*, **59**, 672 (2002).
28. S. Votat, M. Pontié, E. Jaspard, and L. Lebrun, *Energies*, **17**, 247 (2024).
29. M. Shabani et al., *J. Appl. Electrochem.*, **51**, 581 (2021).
30. M. I. González-Sánchez, B. Gómez-Monedero, J. Agrisuelas, J. Iniesta, and E. Valero, *J. Electroanal. Chem.*, **839**, 75 (2019).
31. K. Tyszczuk-Rotko, J. Kozak, and A. Węzińska, *Appl. Sci.*, **11**, 9908 (2021).
32. G. R., T. Venugopal, S. Gopalakrishnan, and S. Sunkar, *Biocatal. Agric. Biotechnol.*, **16**, 400 (2018).
33. S. F. Mbokou, I. K. Tonle, and M. Pontié, *J. Appl. Electrochem.*, **47**, 273 (2017).
34. D. Lu, H. Zou, R. Guan, H. Dai, and L. Lu, *Polym. Bull.*, **54**, 21 (2005).
35. R. M. N. Kalla, M-R. Kim, and I. Kim, *Ind. Eng. Chem. Res.*, **57**, 11583 (2018).
36. B. Roshanravan, H. Younesi, M. Abdollahi, M. Rahimnejad, and S. H. Pyo, *Fuel*, **312**, 122962 (2022).
37. M. Shabani et al., *Renew. Energy*, **179**, 788 (2021).
38. A. Somrani et al., *Ionics*, **27**, 3169 (2021).
39. A. C. Ramdane, F. Guenfoud, and C. Bouraada, *React. Kinet. Mech. Catal.*, **136**, 491 (2023).
40. M. Sbaï, H. Essis-Tome, U. Gombert, T. Breton, and M. Pontié, *Sens. Actuators B Chem.*, **124**, 368 (2007).
41. C. Berríos, J. F. Marco, C. Gutiérrez, and M. S. Ureta-Zañartu, *Electrochim. Acta*, **54**, 6417 (2009).
42. M. Pontié et al., *Electroanalysis*, **23**, 433 (2011).
43. A. García-Miranda Ferrari, C. W. Foster, P. J. Kelly, D. A. C. Brownson, and C. E. Banks, *Biosensors*, **8**, 53 (2018).
44. G. Deffo et al., *Sens. Int.*, **2**, 100126 (2021).
45. S. Nasraoui, S. Ameur, A. Al-Hamry, M. Ben Ali, and O. Kanoun, *Sensors*, **22**, 833 (2022).
46. Q. Liang et al., *Int. J. Electrochem. Sci.*, **14**, 7178 (2019).
47. L. Sun et al., *Microchem. J.*, **182**, 107879 (2022).
48. S. Abdi et al., *Monatshefte Für Chem. - Chem. Mon.*, **154**, 563 (2023).
49. P. Shi et al., *Arab. J. Chem.*, **13**, 1040 (2020).
50. Y. Liu, K. Yan, B. Wang, C. Yang, and J. Zhang, *J. Electrochem. Soc.*, **164**, B776 (2017).
51. S. Chen et al., *Ecotoxicol. Environ. Saf.*, **191**, 110194 (2020).
52. S. E. Baghbamidi et al., *Chin. J. Catal.*, **34**, 1869 (2013).
53. M. Pontie, E. Jaspard, C. Friant, and J. Kilani, *Biocatal. Agric. Biotechnol.*, **22**, 101376 (2019).
54. S. Mani and R. N. Bharagava, *Reviews of Environmental Contamination and Toxicology Volume 237, Reviews of Environmental Contamination and Toxicology.*, ed. W. P. De Voogt (Springer International Publishing, Cham) Vol. 237, 71 (2016).
55. S. J. Kwak et al., *PeerJ*, **12**, e17442 (2024).
56. H. Fan et al., *Environ. Sci. Pollut. Res.*, **30**, 38775 (2022).
57. E. Wudarska et al., *C. R. Chim.*, **18**, 993 (2015).